Experimental examination of a method to estimate temporal effect by neutrons and γ -rays on scintillation light in scintillator-based soft x-ray diagnostic of experimental advanced superconducting tokamak and large helical device

Review of Scientific Instruments

Experimental examination of a method to estimate temporal effect by neutrons and γ-rays on scintillation light in scintillator-based soft x-ray diagnostic of experimental advanced superconducting tokamak and large helical device

Cite as: Rev. Sci. Instrum. **90**, 013507 (2019); https://doi.org/10.1063/1.5054325
Submitted: 30 August 2018 • Accepted: 08 January 2019 • Published Online: 31 January 2019

T. Bando, S. Ohdachi, R. J. Zhou, et al.

Review of Scientific Instruments

AIP Publishing

Review of Scientific Instruments ARTICLE scitation.org/journal/rsi

Experimental examination of a method to estimate temporal effect by neutrons and γ-rays on scintillation light in scintillator-based soft x-ray diagnostic of experimental advanced superconducting tokamak and large helical device

Cite as: Rev. Sci. Instrum. 90, 013507 (2019); doi: 10.1063/1.5054325
Submitted: 30 August 2018 • Accepted: 8 January 2019 •
Published Online: 31 January 2019

T. Bando,[1,a)] S. Ohdachi,[2] R. J. Zhou,[3] G. Q. Zhong,[3] Y. Yuan,[3] L. Q. Hu,[3] and B. L. Ling[3]

AFFILIATIONS

[1]SOKENDAI (The Graduate University for Advanced Studies), 322-6 Oroshi-cho, Toki, Japan
[2]National Institute for Fusion Science, National Institutes of Natural Sciences, 322-6 Oroshi-cho, Toki, Japan
[3]Institute of Plasma Physics, Chinese Academy of Sciences, Hefei 230031, China

[a)]bando.takahiro@qst.go.jp

ABSTRACT

Scintillators, which are more tolerant of neutrons or γ-rays than semiconductors, are a promising candidate for soft X-ray (SX) diagnostics in high neutron flux environments such as JT-60SA or ITER. Although scintillators are tolerant of radiations, neutrons and γ-rays can cause scintillation light and become noise on SX signals. Therefore, a method to estimate the temporal effect by the radiations on SX signals and an appropriate design of the radiation shield based on the estimation are required. In previous studies, it has been proposed for estimating the effect by the radiations to calculate the absorption powers due to SXs, neutrons, and γ-rays in scintillators assuming that amplitudes of scintillation light are proportional to the absorption powers. In this study, an experimental examination of this proposal is conducted in the Experimental Advanced Superconducting Tokamak (EAST). It is shown that the proposal may be valid in the examination of EAST. In addition to results in EAST, initial results of a multi-channel scintillator-based SX diagnostic in the Large Helical Device (LHD) are introduced. Although a scintillator-based SX diagnostic in LHD observes oscillations of SXs by magnetohydrodynamic (MHD) phenomena successfully, the observed temporal effect on SX signals by neutrons or γ-rays is more significant than the expected effect, which is estimated by calculating the absorption powers. One of the possible reasons for the contradiction between the results in EAST and LHD is unexpected γ-rays around the scintillators in LHD. Although the temporal effect by the radiations is significant in the current system of LHD, the degradation of amplitudes of SX signals after the deuterium plasma experiments is not observed with the current level of the fluence. The scintillator-based SX diagnostic in LHD may work as a diagnostic to research MHD instabilities in deuterium plasma experiments without additional maintenance during an experimental campaign by making the pinhole larger or setting an additional radiation shield.

I. INTRODUCTION

A multi-channel soft x-ray (SX) diagnostic has been used as one of the main diagnostics in fusion plasma devices to research magnetohydrodynamic (MHD) equilibria and MHD activities.[1] For this purpose, semiconductors have been used in magnetic confinement devices. However, it will be difficult to use semiconductor detectors near plasmas in future

machines such as JT-60SA or ITER, where the neutron flux around detectors will be severer and will damage semiconductors significantly. Therefore, a well-designed radiation shield must be installed around semiconductors in such environments. Recently, a semiconductor-based SX diagnostic with a well-designed radiation shield has been proposed and developed for the ITER device.[2–4]

Scintillators are also a promising candidate for SX diagnostics in such high neutron flux environments.[5,6] In this type of SX diagnostic, an SX from a plasma is converted to visible light by using a scintillator. The light is then guided to a remote location and measured by using detectors. It is reported that this kind of diagnostic is working well even in high neutron flux environments of NSTX.[7]

The advantage of scintillators is the greater tolerance to radiations compared to semiconductors. According to Ref. 8, the threshold of the fluence by 14 MeV neutrons which decrease amplitudes of signals is different between photo diodes and CsI:Tl scintillators. The threshold fluence for the photodiode is 10^{12} n cm^{-2}, while the threshold fluence for the CsI:Tl scintillator is 10^{15} n cm^{-2}. The threshold of the CsI:Tl scintillator is three orders larger than that of the semiconductor. Therefore, scintillators seem to be able to be used in higher neutron flux environments where semiconductors cannot be used.

Although scintillators are tolerant of radiations, neutrons and γ-rays can cause scintillation light and become noise on SX signals. Therefore, the quantitative estimate of the temporal effect by the radiations on scintillation light and an appropriate design of the shield based on the estimation are required, which is the same as semiconductor-based SX diagnostics.

In previous studies,[9,10] it has been proposed for estimating temporal effect by neutrons and γ-rays to calculate the absorption powers due to SXs, neutrons, and γ-rays in scintillators assuming that amplitudes of scintillation light are proportional to the absorption powers. It was shown that when a thin scintillator (~50 μm) is used with the appropriate γ-ray shield, SXs are absorbed well while the absorbed power by neutrons and γ-rays can be appropriately reduced. However, an experimental examination of this proposal has not been shown in the previous studies.

The Experimental Advanced Superconducting Tokamak (EAST)[11] is a tokamak with superconducting coils. The EAST has neutral beam injectors (NBIs), and then neutrons are expected to be produced with deuterium. Therefore, it is appropriate to examine the proposal in EAST. The result of the examination is reported in this article.

In addition to the experimental examination in EAST, initial results of the multi-channel scintillator-based SX diagnostic in the Large Helical Device (LHD) are introduced. In LHD, semiconductor-based SX diagnostics had been used in hydrogen plasma experimental campaigns.[12] However, for deuterium plasma experimental campaigns of LHD, which started from March 2017, semiconductor-based SX diagnostics were removed because large amounts of neutrons damage semiconductors and then degrade the quality of signals from semiconductors. Instead of semiconductor-based SX diagnostics, a scintillator-based SX diagnostic has been developed[9,10] and has started to work in deuterium plasma experiments of LHD.

This article is organized as follows: In Sec. II, the result of the experimental examination of the proposal in EAST is explained in detail. In Sec. III, the initial results of the multi-channel scintillator-based SX diagnostic in deuterium plasma experiments of LHD are introduced. The summary is described in Sec. IV.

II. EXPERIMENTAL EXAMINATION OF PROPOSAL TO ESTIMATE TEMPORAL EFFECT BY NEUTRONS OR γ-RAYS IN EAST

In EAST, the examination is conducted by comparing signals from two channels of the scintillator-based SX diagnostic. Figure 1 shows a schematic view of the system. The system views plasmas tangentially in the midplane. In the system, SXs, neutrons, and γ-rays from plasmas cause scintillation light. Here, a P47 scintillator (50 μm in thickness), made by ProxiVision, is used as the scintillator. The chemical formula of P47 is Y_2SiO_5:Ce,Tb in this study. The pinhole and Be foil are set for SXs. The size of the pinhole is ϕ 5 mm. The Be foil (12 or 13 μm in thickness) on the pinhole is for cutting low energy photons, whose energy is less than 1.3 keV, from plasmas. The distance from the plasma core to the pinhole is approximately 2.5 m. The distance from the pinhole to the scintillator is approximately 0.2 m. The scintillation light emitted from the scintillator is converged by lenses and transferred by optic fibers. Then, the light is detected by using H10723-210 Photo Multiplier Tube (PMT) modules, made by HAMAMATSU Photonics. The wavelength of the highest sensitivity of the PMT is about

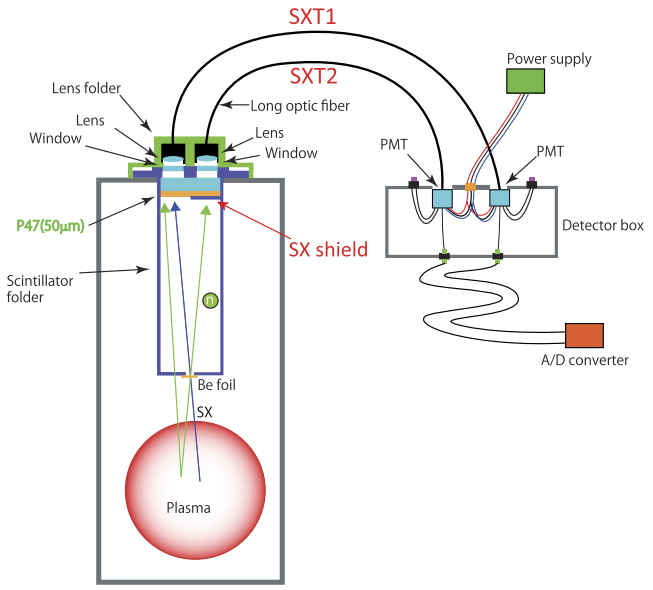

FIG. 1. Schematic view of a system including two SX channels with a P47 scintillator in EAST. One of the two channels (SXT1) detects SXs, neutrons, and γ-rays. The SXT1 is viewing plasmas tangentially in the midplane. The other channel (SXT2) has an SX shield in front of the scintillator and only detects neutrons and γ-rays.

400 nm. This wavelength is almost the same as the strongest emission wavelength of P47.

In this system, one of the two channels (SXT1) detects SXs, neutrons, and γ-rays. The SXT1 views plasmas tangentially in the midplane. However, the other channel (SXT2) cannot detect SXs and only detects neutrons and γ-rays due to the SX shield in front of the scintillator. Here, the SX shield and the folder for the scintillator are made of SS304. The SS304 is a type of stainless steel, which contains chromium (between 18% and 20%) and nickel (between 8% and 10.5%) metals as the main non-iron constituents. The thickness of the SX shield is 1 mm. With this thickness, high energy γ-rays are not attenuated well. In addition, neutrons are not attenuated well because neutrons would enter the space in front of the scintillator through the pinhole and fill it by scattering on the surface of the vacuum vessel without significant loss of its energy. Therefore, with this configuration, the effects of neutrons and γ-rays can be obtained experimentally by comparing signals between SXT1 and SXT2.

The functionality of SX shield is examined in a discharge without NBIs as shown in Fig. 2, which shows signals of (a) the plasma current and the line averaged electron density measured by using the hydrogen cyanide (HCN) interferometer, (b) the total neutron emission rate obtained with a fission chamber, (c) the semiconductor-based SX diagnostic,[13] and (d) the scintillator-based SX diagnostic, respectively. The total neutron emission rate is quite low due to the lack of NBIs. In Fig. 2(d), red-colored and blue-colored signals indicate SXT1 and SXT2, respectively. In this shot, an amplifier is applied to SXT1 because amplitudes of signals from SXT1 are very low. As seen in Fig. 2, the time evolution of signals from SXT1 and semiconductor-based SX diagnostic are quite similar. This observation suggests that SXT1 detects SXs. On the other hand, no response in signals from SXT2 is observed. Therefore, the SX shield seems to work well in this system.

The procedure for the examination of the proposal is as follows. If amplitudes of scintillation light are proportional to the absorption powers in a scintillator, the following equation should be satisfied:

$$\frac{V_{SXT1}}{V_{SXT2}} = \frac{Wsx + Wn + W\gamma}{Wn + W\gamma}. \quad (1)$$

In Eq. (1), V_{SXT1} and V_{SXT2} are output voltages of SXT1 and SXT2, respectively. The Wsx, Wn, and Wγ are the absorption powers due to SXs, neutrons, and γ-rays, respectively. Here, it is assumed that the loss of scintillation light during transmission in the optical system and the sensitivity of PMTs are the same in SXT1 and SXT2. The method for calculation of the absorption powers is based on the previous studies.[9,10] Wsx is calculated by integrating the emitted power into the scintillator by bremsstrahlung. The calculation of bremsstrahlung requires the electron temperature and the electron density in the plasma. The electron density and temperature are calculated using the Thomson scattering measurement, where the core electron temperature and the core electron density are about 3 keV and 4.5×10^{19} m^{-3}, respectively. Although measurement points of the Thomson scattering measurement do not cover the whole plasma, the densities and temperatures in the whole plasma are obtained with an MHD equilibrium, which is calculated by the EFIT code,[14] assuming that the temperatures and densities are the same on each flux surface. Wn and Wγ are calculated with Monte Carlo transport codes[15,16] using a simplified 3D model of EAST.[17] The absorption powers in the scintillator can be obtained with the total neutron emission rate obtained with a fission chamber and the results from the Monte Carlo transport codes.

The examination of the proposal is conducted in the shot shown in Fig. 3, which shows signals of (a) the total neutron emission rate, (b) SXT1, and (c) SXT2, respectively. In this shot,

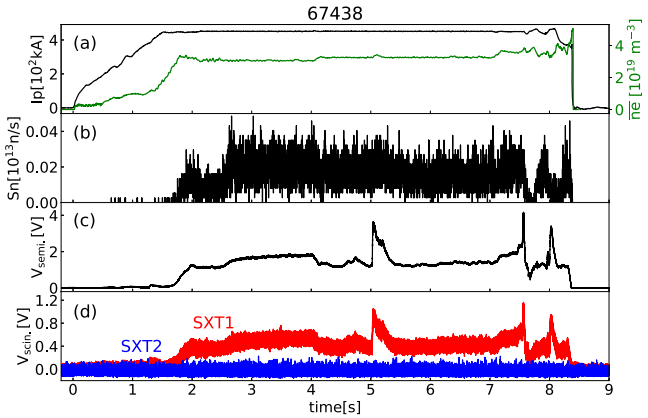

FIG. 2. Signals of (a) the plasma current and the line averaged electron density measured by using the HCN interferometer, (b) the total neutron emission rate obtained with fission chamber, (c) the semiconductor-based SX diagnostic,[13] and (d) the scintillator-based SX diagnostic are shown.

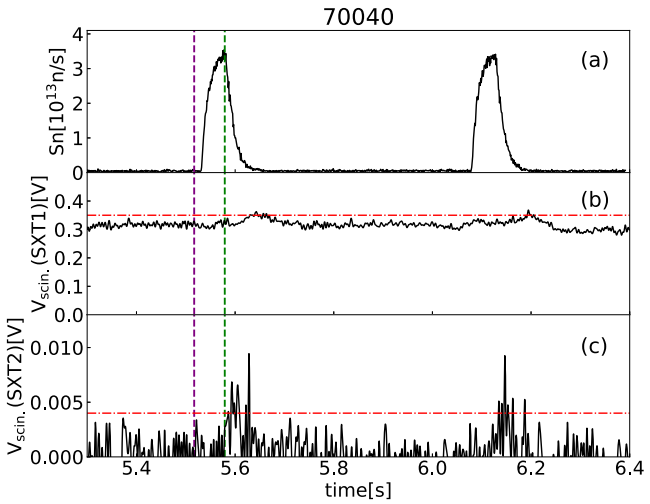

FIG. 3. Signals of (a) the total neutron emission rate, (b) SXT1, and (c) SXT2 are shown. In this shot, NBs are injected repeatedly with intervals. The green dashed line at 5.58 s indicates the peak rate of the neutron emission when the NB is injected. The purple dashed line at 5.517 s indicates the timing of the Thomson scattering measurement. The red dotted-dashed lines indicate the obtained output voltages from SXT1 and SXT2. Here, the low pass filter is applied to SXT1 and SXT2 to cut high frequency noise, in which the frequency is higher than 200 Hz.

NBs are injected repeatedly with intervals. Here, the low pass filter is applied to SXT1 and SXT2 to cut high frequency noise, in which the frequency is higher than 200 Hz. The V_{SXT1}/V_{SXT2} is obtained at the peaks of V_{SXT1} and V_{SXT2} near 5.58 s (the green dashed line) when the NB is injected. Then, the V_{SXT1} and V_{SXT2} are measured as 0.35 V and 0.004 V, respectively, as indicated by the red dotted-dashed lines in Figs. 3(b) and 3(c). The Wsx is calculated with the electron temperature and density obtained by the Thomson scattering measurement at 5.517 s (the purple dashed line). Wn and Wγ are calculated with the total neutron emission rate ~3.3×10^{13} n s^{-1} around 5.58 s when NBs are injected. The difference of the referred time for Wsx, Wn, and Wγ is due to the difference between the timing of the Thomson scattering measurement and the timing of the NBI. Then, Wsx, Wn, and Wγ are calculated as 3.6×10^{-6} W, 1×10^{-8} W, and 1.3×10^{-7} W, respectively. As a result, V_{SXT1}/V_{SXT2} ~ 90 and (Wsx + Wn + Wγ)/(Wn + Wγ) ~ 25. Therefore, the discrepancy, $(V_{SXT1}/V_{SXT2})/\{$(Wsx + Wn + Wγ)/(Wn + Wγ)$\}$, is 3.5.

In this examination, the following component can lead to the difference between V_{SXT1}/V_{SXT2} and (Wsx + Wn + Wγ)/(Wn + Wγ). One of the possible candidates is the contribution to SXs by recombination radiation or impurity radiation. Because only bremsstrahlung is considered for Wsx in this study, the Wsx should be greater with recombination radiation or impurity radiation. Actually, absolute measurements of SX emission in LHD[18] showed that the amplitude of the SX emission is about 10 times greater than an estimation with bremsstrahlung. Therefore, the effects by recombination radiation and impurity radiation reduce the discrepancy. Another possible explanation for the discrepancy is the difference of the sensitivity of the two PMTs. According to comments by Hamamatsu Photonics, the difference can be up to a factor of 2. If these contributions are included, the discrepancy can be estimated from 0.18 to 0.7 when it is assumed that the radiation is enhanced by a factor of 10 due to the impurity radiation and recombination radiation. Because the discrepancy is less than one order, the proposal that calculating the absorption powers in scintillators to estimate the temporal effect by neutrons and γ-rays seems to be valid in this experiment.

III. INITIAL RESULTS OF MULTI-CHANNEL SCINTILLATOR-BASED SX DIAGNOSTIC IN DEUTERIUM PLASMA EXPERIMENTS OF LHD

Figure 4 shows a schematic design of the scintillator-based SX diagnostic in LHD, which is based on Fig. 2 in Ref. 10. This system is essentially a pinhole camera with a scintillator screen. The system views a vertical poloidal cross section of LHD. The size of the pinhole is 2 mm (toroidally) × 6 mm (radially) with the Be foil to cut low energy photons. The thickness of Be foil is 15 μm. Photons whose energies are smaller than 1.3 keV are cut with the foil. Here, the distance from the plasma core to the pinhole is approximately 3.85 m. The distance from the pinhole to the scintillator is approximately 650 mm. Three of the fiber optic plates with a P47 scintillator (FOS) made by ProxiVision are used. The thickness of the P47 scintillator is

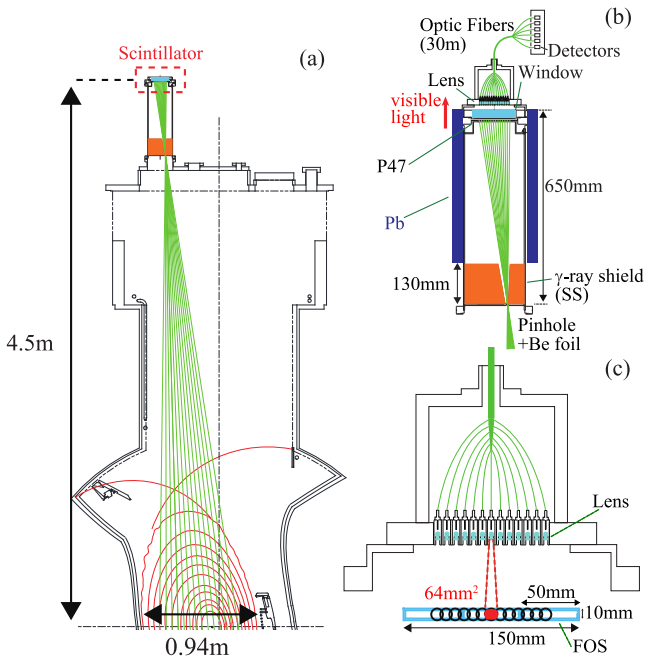

FIG. 4. Schematic design of the scintillator-based SX diagnostic in LHD. (a) Sight lines (green lines) in a vertically elongated cross-sectional view at 3.5U port of LHD are shown. (b) An expanded view of the red box region of the panel (a) is shown. (c) Sensitive areas on the scintillator screen are shown. This figure is based on Fig. 2 in Ref. 10. Reproduced with permission from Bando *et al.*, Rev. Sci. Instrum. **87**, 11E317 (2016). Copyright 2016 AIP Publishing.

35 μm. The difference in thickness of the scintillators between EAST and LHD is due to the difference between each product made by ProxiVision. Each effective area of FOS is 47 mm × 7 mm. The scintillation light is converted by two lenses for one channel. 13 channels can be installed in total with the system. In Fig. 4(c), sensitive areas where the emission light is collected by the lenses are shown. The size of this area is about 64 mm^2. The converged light is transferred by pure silica core optical fibers (30 m in length) to the floor of the experimental hall. The scintillation light is then detected by using a H10723-210 PMT, which is the same as PMTs in EAST described in Sec. II.

The radiation shield is set around the scintillators based on the calculation of the absorption powers[9,10] to reduce the temporal effect by radiations. As shown in Fig. 4(b), the stainless steel layer is set in front of the scintillator as a γ-ray shield. In addition to the front shield, Pb of 4 cm thickness is set around the vacuum vessel.

Note that the SX shield like that of SXT2 in EAST is not installed in the case of LHD because the main purpose of this system is to detect spatial variation of SX emission by MHD instabilities in plasmas of LHD.

The scintillator-based SX diagnostic with seven channels has been installed as the initial configuration in LHD. In the initial configuration, seven PMTs and seven pairs of lenses are used. The lenses are used alternately. The scintillator-based

SX diagnostic started to work in the 19th experimental campaign of LHD. The 19th experimental campaign can be divided into three phases. In the first and third phases, only hydrogen gases are used and neutrons are not produced (hydrogen phase). In the second phase, deuterium gases are used and neutrons are produced (deuterium phase). In the following sections, observations of oscillations on SX signals by MHD phenomena and temporal effect of neutrons or γ-rays on SX signals are discussed.

A. Observation of MHD phenomena

Figure 5 shows (a) SX signals viewing the inner side and the outer side of the plasma, which are obtained with the scintillator-based SX diagnostic, and (b) magnetic fluctuations when m/n = 1/1 locked mode-like instability[19] is observed in the hydrogen phase. The coherent oscillations on SX signals to magnetic fluctuations are clearly observed. In addition, the phases of oscillations of SX signals are opposite between the signals viewing the inner and the outer sides of the plasma. Therefore, it can be said that this system observes variations of radial structure of SX fluctuations by MHD phenomena. Note that the decrease in the amplitudes of SX signals around 4.85 s is due to the sudden decrease in the electron temperature induced by the locked mode-like instability.[19] In addition to the locked mode-like instability, rapid changes of radial profiles of SX signals with core density collapse events[20] are also observed in the hydrogen phase.

Note that coherent oscillation on SX signals to magnetic fluctuations is also observed when MHD modes appear in the deuterium phase. However, the noise by neutrons or γ-rays on SX signals are significant, as described in Sec. III B, and the oscillation on SX signals are not as clear as that in Fig. 5(a).

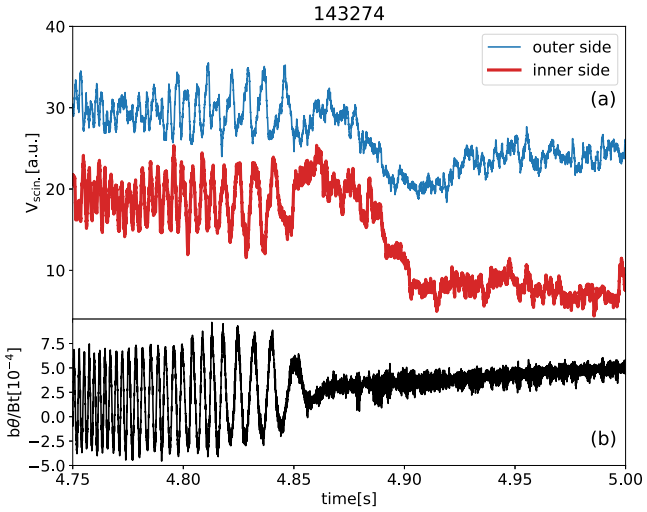

FIG. 5. (a) SX signal viewing the outer side (a blue thin line) and the inner side (a red bold line) of the plasma and (b) magnetic fluctuations in the hydrogen phase are shown. Here, m/n = 1/1 locked mode-like instability[19] is observed.

B. Effect on SX signals by neutrons and γ-rays

Here, the effect by neutrons and γ-rays is examined with dependence of amplitudes of signals from the scintillator-based SX diagnostic on the electron density and temperature. In the examination, the emitted SX power from a plasma to the scintillator through a Be foil is evaluated with the following relational expression:

$$f(\vec{r})_{\text{brems.}} \propto Z_{\text{eff}}^2 n_e n_i (T_e)^{0.5} \exp(h\nu_0/T_e), \tag{2}$$

where $f(\vec{r})_{\text{brems.}}$ is the power of bremsstrahlung emitted from a unit volume in a plasma,[18] Z_{eff} is the effective ion charge, n_e and n_i are the electron and ion density, respectively, T_e is the electron temperature, and $h\nu_0$ is the cutoff energy for photons by the Be foil on the pinhole. Then, in this study, the expected output voltage due to bremsstrahlung, $V_{\text{expected.}}$, is estimated with the following expected equation:

$$V_{\text{expected.}} = F \times G \times \int_{l_c} 1.6 \times Z_{\text{eff}}^2 \left(\frac{n_e}{10^{19}}\right)^2 \left(T_e \times 10^3\right)^{0.5} \times \exp\left(-\frac{h\nu_0}{T_e}\right) \frac{\Delta\Omega}{4\pi} S_p dl_c. \tag{3}$$

Here, the line integration $\int_{l_c} dl_c$ is performed on the sight line of the diagnostic.[9] Here, Z_{eff} is assumed to be 1. It is assumed that $n_e = n_i$, and n_e is assumed to be constant. The unit of n_e is m^{-3}. The electron temperature profile is assumed to be a parabolic one, $T_e(\rho) = T_{e0}(1 - \rho^2)$. ρ is the normalized minor radius. The unit of T_{e0} is keV. $h\nu_0$ is 1.3 keV, which is the cutoff energy of the Be foil. $\Delta\Omega$ is the solid angle from a plasma to the scintillator. S_p is the area of the detector, projected in the plasma through the pinhole. $\frac{\Delta\Omega}{4\pi} S_p$ is evaluated as 3×10^{-10} m^2 in this study, which is the same as in Ref. 9. G is the conversion factor from the absorption power to the output voltage of PMT. Here, G is calculated as 2×10^8 V/W with the absolute photon yield of the scintillator, the energy of photons from the scintillator assuming that the wavelength is 400 nm, the attenuation in the optic fiber, and the sensitivity of the PMT. F is the unexpected attenuation as mentioned in the last paragraph of Sec. III B. F is estimated as 6×10^{-4}.

Figure 6(a) shows the dependence of the amplitude from the scintillator-based diagnostic in the hydrogen phases before (blue) and after (red) the deuterium phase. Here, $V_{\text{scin.}}$ is the output voltage of the SX channel viewing the core of the plasma, n_{e0} is the core electron density, and T_{e0} is the core electron temperature. The black-dashed line is the expected dependence with Eq. (3). The dataset is almost on the black dashed line, and then it is confirmed that SXs are well detected by this diagnostic. Figure 6(b) shows the dependence in the deuterium phase. The colorbar indicates the amount of the total neutron emission rate, Sn, measured by using the neutron flux monitor.[21,22] The black-dashed line is the expected dependence with Eq. (3), which is the same as the black dashed line in Fig. 6(a). When the total neutron emission rate is about 1.5×10^{14} n s^{-1}, which is equal to 1.9×10^7 n cm^{-2} s^{-1} around the scintillators based on the Monte Carlo N-Particle code (MCNP) calculation in the previous study,[10] the clear increase in $V_{\text{scin.}}$ is observed compared with the hydrogen case.

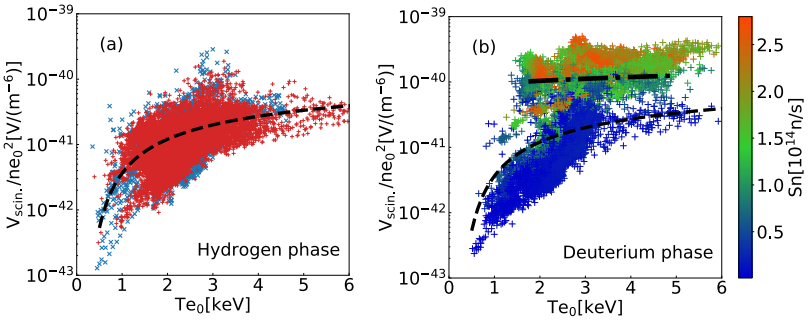

FIG. 6. (a) Dependence of $V_{scin.}/n_{e0}^2$ on T_{e0} in the hydrogen phases before (blue) and after (red) the deuterium phase. (b) Dependence of $V_{scin.}/n_{e0}^2$ on T_{e0} in the deuterium phase. The colorbar indicates the amount of the total neutron emission rate measured by using the neutron flux monitor.[21,22] In figure (a) and (b), the black dashed lines are the expected dependence calculated with Eq. (3). The black dashed dotted line is drawn with the black dashed line and the contribution of the obtained B in Sec. III B assuming that Sn and n_{e0} are 1.0×10^{14} n/s and 1.5×10^{19} m^{-3}, respectively.

In this study, the observed temporal effect by neutrons or γ-rays is evaluated with the following expected equation (4) assuming $n_e = n_i$ and $Z_{eff} = 1$:

$$V_{scin.} = An_e^2(T_e)^{0.5}\exp(-h\nu_0/T_e) + BSn. \quad (4)$$

Here, A and B are factors. The factors can be obtained with the curve fitting using the dataset for Fig. 6(b). Then, the variable B is estimated as 2×10^{-16} V(n/s)$^{-1}$. The validity of the obtained B is examined with an observation of the decrease in $V_{scin.}$, $\delta V_{scin.}$, by the large prompt decrease in Sn, δSn, when helically trapped Energetic-ion driven resistive InterChange modes (EICs)[23] are induced, which induce large loss of helically trapped-energetic-ions and do not change the n_e and T_e significantly. The relation $\delta V_{scin.} \sim B\delta Sn$ is observed with the EIC and then B is validated. The black dashed-dotted line in Fig. 6(b) is drawn with the black dashed line and the contribution of the obtained B, assuming that Sn and n_{e0} are 1.0×10^{14} n/s and 1.5×10^{19} m^{-3}, respectively. The black dashed-dotted line seems to be on the dataset. The obtained B is several hundred times as high as the expected value estimated by calculating absorption powers, which is inconsistent with the results in EAST shown in Sec. II. One of the possible reasons for the contradiction between the results in EAST and LHD is the unexpected γ-rays from materials near the scintillators. A further study is required for the examination.

Although the temporal effect on SX signals is observed, the degradation of amplitudes of SX signals in the hydrogen phase after the deuterium phase is not observed with the current level of the fluence, which is about 4.7×10^{11} n cm^{-2} around the scintillators estimated with the total neutron yield in the 19th experimental campaign of LHD, as shown in Fig. 6(a). Therefore, it may be said that the scintillator-based SX diagnostic can be used during an experimental campaign without additional maintenance in LHD. The temporal effect of neutrons or γ-rays can be reduced by making the pinhole larger or setting an additional radiation shield. Here, the effect of a larger pinhole to Wsx can be calculated with the method described in Ref. 10. SX signals with the reduced temporal effect by radiations may be obtained with these modifications, and SX signals may detect MHD instabilities well in deuterium plasma experiments. In this study, other radiation damage effects, such as the time response of scintillation light to SXs, are not investigated. The investigations will be future work.

Note that the observed output voltage from the scintillator-based SX diagnostic is much smaller than the expected values calculated with the absorption power due to SXs (SX is assumed to be bremsstrahlung), the absolute photon yield of P47, the energy of photons from P47, the transmission rate of the optic fibers, and the sensitivity of PMTs in LHD and EAST. These lower amplitudes may be due to large loss of scintillation light between the FOS and the lenses. An additional examination is also required on this issue.

IV. SUMMARY

In this article, the experimental examination of the proposal, which is suggested in previous studies,[9,10] to estimate the temporal effect by neutrons and γ-rays is conducted in EAST. The suggested proposal is to estimate the temporal effect by calculating the absorption powers in scintillators. In the examination of EAST, the ratio of the output voltages of the two channels of scintillator-based diagnostic and the ratio calculated with the absorption power by SXs, neutrons, and γ-rays are compared. Here, one of the two channels has the SX shield in order to evaluate the contributions by neutrons and γ-rays only. If the ratios are of the same order, the proposal should be valid. As discussed in Sec. II, it is shown that the proposal may be valid in the examination of EAST. In addition to results in EAST, initial results of multi-channel scintillator-based SX diagnostic in LHD are also introduced. Although the scintillator-based SX diagnostic in LHD observes oscillations of SXs by MHD phenomena successfully, the observed temporal effect on SX signals by neutrons or γ-rays is more significant than the expected effect, which is estimated by calculating the absorption powers. One of the possible reasons for the contradiction between the results in EAST and LHD is unexpected γ-rays around the scintillators in LHD. Further study is required for the examination.

On the other hand, no degradation on amplitudes of SX signals from the scintillator-based SX diagnostic is observed after deuterium plasma experiments in LHD. Although investigations regarding reasons for the significant temporal effect on SX signals by neutrons or γ-rays are required, the scintillator-based SX diagnostic in LHD may work as a diagnostic to research MHD instabilities in deuterium plasma experiments without additional maintenance during an experimental campaign by making the pinhole larger or setting an additional radiation shield. This result suggests that there

is a possibility that the scintillator-based SX diagnostic can work without additional maintenance in a high neutron flux environment, such as the ITER device, with an appropriate radiation shield.

ACKNOWLEDGMENTS

This paper is the result of many fertile suggestions from Professor Emeritus K. Toi, Professor T. Nishitani, Professor M. Isobe, Dr. K. Ogawa, Dr. Y. Duan, and Dr. K. Chen. This work was supported by NIFS budget code ULPP021, 028 and was also partially supported by the Ministry of Education, Science, Sports and Culture Grant-in-Aid for Scientific Research No. 26249144, by the JSPS-NRF-NSFC A3 Foresight Program (NSFC: No. 11261140328, NRF: No. 2012K2A2A6000443), and NIFS/NINS under the project of Formation of International Scientific Base and Network.

REFERENCES

[1]L. C. Ingesson, B. Alper, B. J. Peterson, and J. C. Vallet, Fusion Sci. Technol. **53**(2), 528 (2008).
[2]S. Qin *et al.*, Fusion Eng. Des. **112**, 169 (2016).
[3]L. Hu *et al.*, Fusion Sci. Technol. **70**, 112 (2016).
[4]L. Hu *et al.*, Nucl. Instrum. Methods Phys. Res., Sect. A **870**, 50 (2017).
[5]D. Stutman *et al.*, Rev. Sci. Instrum. **76**, 023505 (2005).
[6]D. Stutman *et al.*, Rev. Sci. Instrum. **83**, 10E535 (2012).
[7]L. F. Delgado-Aparicio, D. Stutman, K. Tritz, and M. Finkenthal, Rev. Sci. Instrum. **75**, 4020 (2004).
[8]T. Iida *et al.*, J. Nucl. Sci. Technol. **27**, 651 (1990).
[9]T. Bando, S. Ohdachi, and Y. Suzuki, Plasma Fusion Res. **10**, 1402090 (2015).
[10]T. Bando, S. Ohdachi, and Y. Suzuki, Rev. Sci. Instrum. **87**, 11E317 (2016).
[11]B. N. Wan *et al.*, Nucl. Fusion **57**, 102019 (2017).
[12]S. Ohdachi *et al.*, Fusion Sci. Technol. **58**, 418 (2010).
[13]K. Chen *et al.*, Rev. Sci. Instrum. **87**, 063504 (2016).
[14]L. L. Lao *et al.*, Nucl. Fusion **25**, 1611 (1985).
[15]X-5 Monte Carlo Team, MCNP–A general N-particle transport code, version 5, volume I: Overview and theory, LA-UR-03-1987, Los Alamos National Laboratory, USA, 2003.
[16]T. Sato *et al.*, J. Nucl. Sci. Eng. **50**, 913 (2013).
[17]Z. M. Hu *et al.*, Rev. Sci. Instrum. **85**, 11E417 (2014).
[18]S. Ohdachi, Ph.D. thesis, Nagoya University, 2003, p. 48.
[19]Y. Takemura *et al.*, Nucl. Fusion **52**, 102001 (2012).
[20]S. Ohdachi *et al.*, Nucl. Fusion **57**, 066042 (2017).
[21]M. Isobe *et al.*, Rev. Sci. Instrum. **85**, 11E114 (2014).
[22]T. Nishitani *et al.*, Fusion Eng. Des. **123**, 1020 (2017).
[23]K. Ogawa *et al.*, Nucl. Fusion **58**, 044001 (2018).